ACS APPLIED MATERIALS & INTERFACES

Research Article

www.acsami.org

Click-In Ferroelectric Nanoparticles for Dielectric Energy Storage

Brian C. Riggs,* Ravinder Elupula, Caroline Rehm, Shiva Adireddy, Scott M. Grayson, and Douglas B. Chrisey*

Tulane University, 6232 St. Charles Ave, New Orleans, Louisiana 70118, United States

Supporting Information

ABSTRACT: Polymer−ceramic nanocomposites have been thoroughly investigated previously for high energy storage devices. However, the increase in performance of these nanocomposites has proven to be significantly lower than predicted values. Through surface functionalization of high dielectric constant nanoparticles (NP), the flaws that reduce composite performance can be eliminated to form high energy density composite materials. Functionalization methods utilize high throughput printing and curing techniques (i.e., inkjet printing and xenon flash lamp curing) that are crucial for rapid adoption into industrial production. (Ba,Ca) (Zr,Ti)O_3 NPs (50 nm) are synthesized through the solvothermal method and functionalized with alkene terminated methoxysilanes. A thiol−ene monomer ink system, PTD3 [pentaerythritol tetrakis (3-mercaptopropionate) (PEMP, P), 1,3-Diisopropenylbenzene (DPB, D), 2,4,6-Triallyloxy-1,3,5-triazine (TOTZ, T)], is used as a high breakdown polymer matrix. Neat polymer, alkene terminated NP−polymer composites, and hydrophilic, TBAOH functionalized NP−polymer composites were spin coated onto both copper laminated glass slides and printed onto copper substrates in 1 cm^2 patterns for testing. Alkene functionalized NPs increased the breakdown strength by ∼38% compared to the nonfunctionalized NPs. Functionalized NPs increased both the breakdown strength and dielectric constant compared to the neat polymer, increasing the energy density nearly 3-fold from 13.3 to 36.1 J·cm^{-3}.

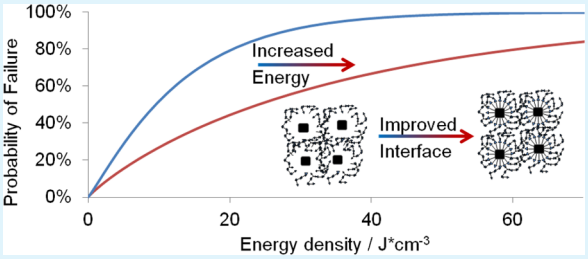

KEYWORDS: *click-chemistry, energy storage, printed electronics, photonic curing, nanocomposite*

1. INTRODUCTION

With recent focus on renewable energy production, high energy, high power density electrical storage methods have become a necessity to improve grid scale load leveling for instantaneous and periodic fluctuations.[1−4] Over the next 20 years, the global energy demands are expected to increase over 50% to nearly 600 quadrillion BTU, increasing the demand for not only energy generation, but also energy storage.[5−7] Current technologies, such as Pb-acid[8,9] or Li-Ion batteries,[10−14] have gained significant interest due to their high gravimetric energy densities; however, next generation energy storage must have a large capacity, be capable of rapid charge/discharge, and have superior wear properties including high cycling and charge retention.[15−19] Solid state dielectric capacitors are the only energy storage method that have intrinsically high power densities and the desirable wear properties, making them an attractive candidate for further development.[20−27]

The major drawback for dielectric capacitors is their relatively low energy density. The energy density of dielectric capacitors is approximately 3 orders of magnitude less than that of Li-ion technologies. Improving the energy density of dielectric capacitors has been of particular interest over the past 10 years focusing on high dielectric constant ceramics,[26−39] high breakdown polymers,[40−51] and composites of these materials.[24,32,52−61] Research on dielectric capacitors aims to improve the two material properties that dictate the energy density of a device (i.e., dielectric constant and breakdown field). From the volumetric energy eq 1, it is clear that the most significant contribution is from the breakdown field, E_b, which increases the energy density by its square. Hence, the majority of current research is in polymer dielectrics, focusing on maximizing the breakdown field in exchange for a lower dielectric constant.

$$\mathrm{ED}_v = \frac{1}{2}\varepsilon_o\varepsilon_r E_b^2 \tag{1}$$

Ultimately, both the dielectric constant and breakdown field need to be improved in order to obtain energy densities that rival current battery technologies. By combining high dielectric constant ceramic NPs with high breakdown strength polymers, significant progress has been made in increasing the energy density of dielectric capacitors.[24,53,62−67] However, the interface between high permittivity NP and low permittivity polymer matrix leads to an incoherent interface, creating a charge concentration region, which ultimately lowers the breakdown strength and lowers the energy density. These defects are the most significant factor in reducing device performance, even at low volume fraction of NPs. Because of the importance of eliminating the interfacial defects, significant work has been put

Received: May 14, 2015
Accepted: July 27, 2015
Published: July 27, 2015

DOI: 10.1021/acsami.5b04158
ACS Appl. Mater. Interfaces 2015, 7, 17819−17825

Scheme 1. Process of Nanoparticle Functionalization and Incorporation into the Polymer Matrix

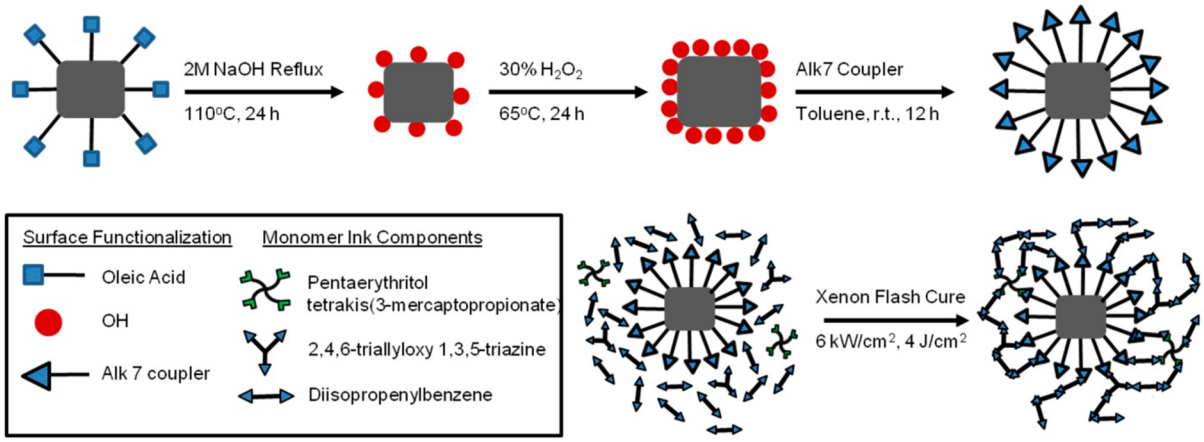

into engineering the interface between NP and polymer including using Van der Waal attraction, hydrogen bonding, and polymer grafting to associate the polymer matrix with the ceramic NPs.[60−63,66]

Direct covalent bonding between the high dielectric ceramic particle and high breakdown polymer matrix is the most direct way of eliminating the incoherent interface that diminishes the energy storage potential of nanocomposites. By covalently attaching alkene terminated methoxysilanes onto ceramic NPs, NPs can be directly connected into a thiol-click based polymer matrix creating a strongly bound, coherent interface between ceramic NP and polymer network, eliminating defects that would reduce the breakdown strength. Thiol−ene polymers have been proven as a potential versatile high breakdown polymer matrix due to their ease of handling,[68] potential for high throughput processing,[69] and high degree of cross-linking. From the design of materials perspective, versatility of click chemistry allows a large library of functional groups, structures, and varieties of chemistry to be assembled in user defined structures. The relatively low energies necessary to cure without the need for photoiniators decreases processing time, improving production throughput and combinatorial testing. The click mechanism of curing allows for the careful control of polymer structure. Because of this, thiol−ene polymers have begun to become of interested for dielectric applications.[68−70] As the NP surface functionalization matches the chemistry of the polymer system, the resulting solution can be treated as a well dispersed NP ink, allowing it to be printed and cured using high throughput methods such as inkjet printing and photonic processing, facilitating its adoption into industrial production. The following paper will describe a novel approach to eliminating the incoherent interface between ceramic NPs and polymer matrix for dielectric nanocomposites, allowing for simultaneous increase in both dielectric constant and breakdown strength, leading to a dramatic increase in energy density.

2. EXPERIMENTAL SECTION

2.1. Nanoparticle Growth, Functionalization, and Characterization. High dielectric constant BZCT NPs [$(Ba_{0.7}Ca_{0.3})$ $(Zr_{0.2}Ti_{0.8})$-O_3] were grown for 16 h using a modified solvothermal method.[71] Barium nitrate and *n*-Decanol were obtained from Alfa Aesar (Ward Hill, MA). Calcium acetate, Titanium butoxide, Zirconium isopropoxide, oleic acid, and tetrabutyl ammonium hydroxide were obtained from Sigma-Aldrich (St. Louis, MO). Sodium hydroxide was obtained through VWR (Radnor, PA). After growth, NPs were washed in a mixture of ethanol and acetone and centrifuged at 6000 rpm for 10 min to collect the particles. TEM (FEI G2 F30 Tecnai TEM) was used to confirm particle size and distribution. XRD, Raman Spectroscopy, and XPS were used to determine crystal structure, tetragonality, and elemental confirmation, respectively.

Scheme 1 summarizes the functionalization and composite curing process. BZCT NPs were refluxed for 24 h at 110 °C in 2 M NaOH aqueous solution to remove oleic acid chains through ester saponification. The resulting solution was sequentially washed (ultrasonicated for 10 min, centrifuged for 20 min at 11 000 rpm) in toluene, tetrahydrofuran (THF), and methanol. After the final wash step, particles were magnetically stirred and heated at 65 °C for 24 h in a 30% peroxide solution to increase hydroxide surface functionalization.[58] The particles were washed as previously described. The coupling agent 7-octenyltrimethoxysilane (Alk7) was obtained from Gelest, Inc. (Arlington, VA). 500 mg of Alk7 was reacted at room temperature with ∼80 mg of hydroxilated NP in toluene under nitrogen overnight. These particles were washed as described above. As a control, as-grown BZCT NPs were reacted with 1 M TBAOH/DI H_2O overnight at 50 °C to form hydrophilic BZCT. These samples were designated BZCT TBAOH and were used as a negative control, forming a defined incoherent interface between the particle and polymer matrix.

FTIR was used to confirm the covalent attachment of active alkene groups to the surface of the NP. The C═C bond at 1650 cm^{-1}, the ═C—H bond around 1100 cm^{-1}, and the C═C—H bond at 3100 cm^{-1} were used as confirmation of alkene functionalization. TGA weight loss data was used to determine the total amount of coupling agent on the NPs and calculate the average attachment density. Curves were normalized to the weight at 200 °C, as to not include the water loss in the calculation. Decomposition of surface alkene groups did not start until 250−300 °C.

2.2. Dielectric Inks. Supporting Information (SI) Figure S1 shows the chemical structure of all monomers used in the creation of the UV curable ink. All monomer solutions were obtained from Sigma-Aldrich (St. Louis, MO). Pentaerythritol tetrakis(3-mercaptopropionate) (6 mol %, PEMP), 1,3 Diisopropenylbenzene (82 mol %, DPB), and 2,4,6-triallyloxy 1,3,5-triazine (11 mol %, TOTZ) were combined as previously described to form the PTD3 monomer ink.[69] For NP−polymer composite inks, 6 wt % (1 vol %) of hydrophilic (BZCT-TBAOH) and alkene functionalized (BZCT Alk7) NPs were mixed into thiol−ene PTD3 inks and ultrasonicated for 5 min to form a well-dispersed solution. For testing, 1 in^2 samples were spin coated onto copper laminated glass substrates (0.7 mL, 500 rpm 20 s, 2000 rpm 45 s) and 1 cm^2 layers of ink were printed onto 30 μm copper foil substrates (Oak Mitsui, Hoosick Falls, NY). Inkjet samples were printed using a Fujifilm Dimatix 2800 Inkjet printer with 10 pL print heads using a standard inkjet waveform with the voltage adjusted to control the drop velocity and volume to approximately 8 m/s and 6 pL, respectively.

DOI: 10.1021/acsami.5b04158
ACS Appl. Mater. Interfaces 2015, 7, 17819−17825

2.3. Xenon Flash Lamp Curing. The Pulseforge 1300 (Novacentrix, Austin, TX) was used to cure the printed films using the pulse profile is as follows: 450 V, 3000 μs, 5 μp, 50% duty cycle. The curing fluence and intensity were 4 J/cm^2 and 6 kW/cm^2 respectively. Films were cured in groups of 10 pulses at 1 Hz until they demonstrated mechanical stability through a scratch test. All films were cured after 30 pulses. A multimeter was used to confirm the formation of an electrically insulating layer. Wiping the films with acetone without any material loss demonstrated chemical stability.

2.4. Morphological Characterization. Optical microscopy was used to inspect for wrinkles, cracks, pinholes, other flaws, and pattern registry. Surface morphology, cross section, and film thickness were examined with a Hitachi S-4800 FESEM.

2.5. Dielectric and Energy Storage Characterization. 500 μm diameter gold electrodes were sputtered onto cured polymer films for testing. Dielectric properties were tested using an Agilent 4294a impedance analyzer (Agilent Technologies, St. Clara, CA) with the frequency range 100 Hz to 1 MHz using a two terminal set up. 4−5 electrodes were measured for each sample. Breakdown measurements were made using Radiant Technologies' (Albuquerque, NM) Premier II Ferroelectric tester with 10 kV amplifier (Trek Inc., Lockport, NY). Breakdown strength was determined by taking repeated leakage current measurements with a 500 ms soak and 1000 ms read time. The voltage was increased according to the sample thickness to obtain a 0.1 MV/cm field increase each test. Failure was considered when the leakage current of 1 mA was measured. Breakdown measurements were conducted 8−12 times in order to perform a Weibull analysis. The resulting Weibull distribution was used in the linear dielectric energy eq 1 to calculate the volumetric energy density distribution.

3. RESULTS AND DISCUSSION

3.1. Synthesis of BZCT Nanoparticles. Figure 1 shows TEM images of the NPs with an average size of ~41.7 nm.

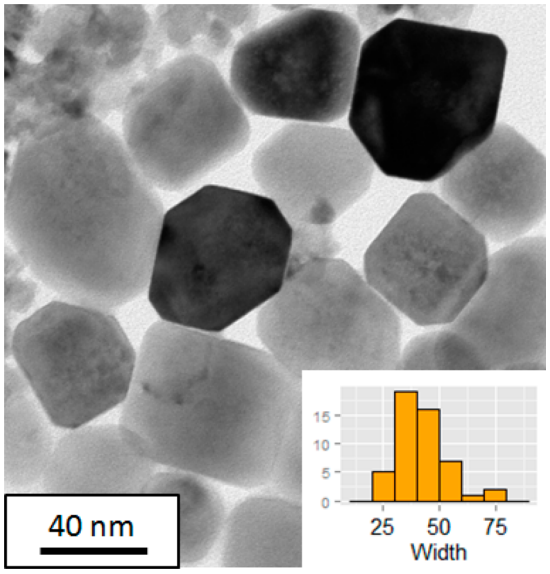

Figure 1. TEM images of 50 nm BZCT nanoparticles. Particles show mostly cubic morphology with rounded corners. Few particles have spherical morphologies. Inset: Distribution of particle size. n = 50.

Particles exhibit mostly cubic morphology with some corners unevenly cut off. Few NPs had spherical morphologies. The inset of Figure 1 shows the size distribution of the synthesized NPs. The average particle side length is 41.7 nm. Less than 25% of particles had side lengths of >50 nm. The narrow particle distribution produced by the solvothermal growth method is a significant benefit for inkjet printing which can face a number of issues if particles are too large including complete clogging, uneven drop formation, and printhead misfiring. SI Figure S2 shows the XRD scan, Raman spectrum, and XPS spectrum of the grown BZCT NPs. SI Figure S2a shows phase pure perovskite BZCT. Raman spectroscopy (SI Figure S2b) confirms tetragonality of the perovskite phase with peaks present at 304 cm^{-1}. XPS analysis (SI Figure S2c) confirms the presence of all 5 elements in the BZCT ceramic.

3.2. Refunctionalization of Grown BZCT Nanoparticles. Figure 2 shows the FTIR spectrum for each step in the

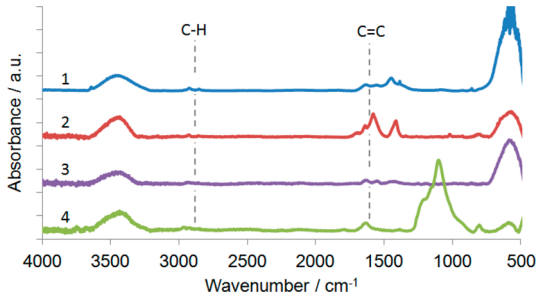

Figure 2. FTIR spectra for the refunctionalization process from oleic acid to alkene couplers. 1) As-grown BZCT NP. 2) NaOH refluxed NP. 3) Peroxide reacted NP. 4) Alkene coupled NP.

refunctionalization process for solvothermally grown BZCT NPs. As-grown NPs show oleic acid peaks at 1650, 2800−3000, and 3600 cm^{-1}. The large, broad peak from 400 to 600 cm^{-1} is due to the bulk absorbance of BZCT NPs. The NaOH reflux spectrum clearly shows the removal of oleic acid during the 2 M NaOH reflux due to the loss of the C═C (1650 cm^{-1}) and C—H (2800−300 cm^{-1}) peaks. The return of these peaks in Alk7 coupling shows that the surface alkene functionalities were successfully attached.

Figure 3 shows the TGA analysis for the refunctionalization of the as-synthesized particles, BZCT OL. Weight loss in BZCT

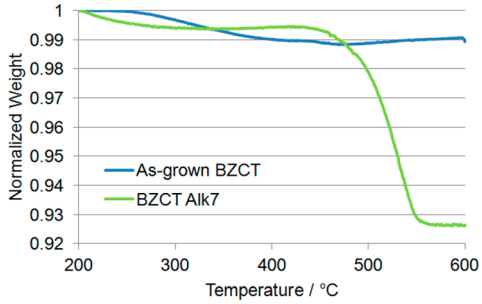

Figure 3. TGA of oleic acid BZCT nanoparticles refunctionalized with Alk7 coupling agent.

Alk7 was 8% greater than as-grown BZCT NPs. Using the weight loss and molecular weight of the attached organic molecules (oleic acid or Alk7), the organic compound chain density and average number of chains per particle can be calculated (SI Table S1). The calculation shows an increase in chain density and the total number of chains per NP from oleic acid (~10 000) to Alk7 (~74 000). This is attributed to the peroxide reaction step that increases the number of hydroxyl groups on the NP surface, giving more sites for the coupling reaction to occur. The calculation is important for future nanocomposite design, as it would allow for adjustments to be made in the monomer ink composition to match the number of thiol and alkene groups, assuring that there is a maximum

DOI: 10.1021/acsami.5b04158
ACS Appl. Mater. Interfaces 2015, 7, 17819−17825

degree of cross-linking in the final composite with minimal free ends. By introducing 1 vol % (~6 wt %) of functionalized NPs into the polymer matrix, the ratio of available cross-linking bonds vs linear bonds increases from 0.36 to 1.25 × 10.[21] Due to the large number of potential cross-linking bonds on the NP (~74 000), even a small loading of powder drastically increases the degree of cross-linking in a mostly linear polymer such as PTD3.

3.3. Energy Storage Properties. *3.3.1. Spin-Coated Samples.* To determine the effect of the interface on breakdown strength, neat PTD3, BZCT TBAOH-PTD3 composite, and BZCT Alk7-PTD3 samples were spin coated onto copper laminated glass slides and cured using the pulse setting detailed above. The BZCT TBAOH particles were considered to form a nonbonding, incoherent interface with the resulting polymer matrix due to the drastic difference in polarity between the OH shell and the PTD3 matrix. BZCT Alk7 NPs undergo a click reaction and bond directly with the polymer matrix. SEM cross sections (SI Figure S3) of the three spin coated samples show highly dense films 1.5−2 μm thick. Optical microscopy showed mostly uniform films with no cracks or wrinkles. Due to the lamination process of the copper onto glass substrates, there are minor fluctuations in substrate height resulting in local variation of thickness.

Figure 4 includes the Weibull distributions for the spin coated samples. The BZCT TBAOH-PTD3 nanocomposite

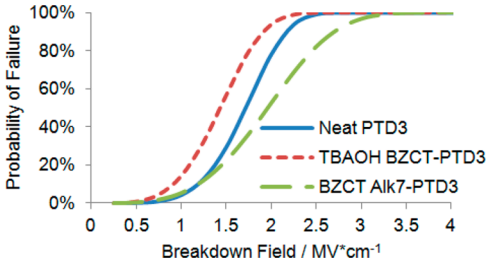

Figure 4. Weibull distribution for spin-coated neat PTD3 (solid line), TBAOH functionalized composite (dotted line), and ALK7 functionalized composite films (dashed line).

show a significant decrease in the breakdown field compared to the neat PTD3. This is attributed to the distinct incoherent interface between the particle and polymer matrix, forming an artificial porosity in the polymer film. The scale parameter (alpha, the characteristic breakdown field) decreased by 15% when the BZCT TBAOH particles were introduced compared to the neat PTD3 polymer film (1.84 to 1.56 MV·cm^{-1}). In contrast, BZCT Alk7 NPs increased the breakdown by 17% (1.85 to 2.16 MV·cm^{-1}). Because creating a coherent interface between NP and matrix would only maintain the breakdown strength of the polymer at best, the observed increase in breakdown field for the presented composite system is attributed to an increasing in the degree of cross-linking for PTD3 films. This is supported by the reduction in swell ratio when NPs were added (PTD: 1.126 and 1%NP-PTD3:1.001). As described by Yuan et al.,[72] increasing the degree of cross-linking decreases the effective free volume of the polymer film leading to an increase in breakdown field. The functionalized NPs increase the degree of cross-linking by adding ~74 000 bonding sites as suggested above by the chain density and chains per particle..

3.3.2. Inkjet Printed Films. One vol % 50 nm BZCT Alk7-PTD3 ink was printed into 1 cm test squares to determine the composite dielectric, breakdown, and energy storage properties. The inkjet printing behavior of the composite was similar to that of neat PTD3. Drops formed short tails with a minor satellite that followed behind the main drop. No changes to the voltage or waveform were necessary due to the low loading fraction of NPs. Optical micrographs (SI Figure S4) show minor defects in printing that were due to incomplete surface treatment with an acetone wipe necessary to increase the contact angle between ink and substrate. The nanocomposite film appears significantly more matte than the neat polymer film due to the change in optical absorption from the NPs as well as increased surface roughness.

The frequency dependent dielectric constant studies can be found in Figure 5a. There are two interesting notes about the dielectric constant when compositing with the ceramic NP. First, the increase in dielectric constant is above the predicted composite dielectric constant according to the rule of logarithmic mixing. Although the rule of mixing is sufficient at median loadings, at the highly concentrated and highly dilute (such as 1 vol %) levels, it is a poor approximation. An increase from 15 to 17 is a small change however it does lend to an increase the overall energy storage properties. The second attribute of note is the decreased frequency dependence of the dielectric constant that increases the potential range of applications for this dielectric composite. This is attributed to the increased ceramic loading that is known for low frequency dependence over a wide range of frequencies as well as the increase in cross-linking, limiting polymer chain mobility.

As was seen in the spin-coated samples, there was a significant increase in the breakdown strength due to the addition of the alkene functionalized NPs. Figure 5b shows the Weibull distributions of the neat PTD3 material and the printed nanocomposites. As can be seen, the inclusion of cross-linking NPs increases the characteristic breakdown by 50% from 4.4 MV/cm to 6.7 MV/cm. This change in breakdown results in a drastic increase in energy storage. The increase in

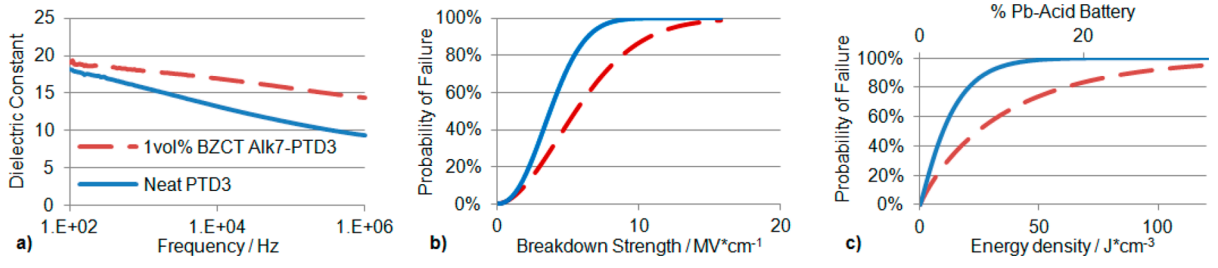

Figure 5. (a) Frequency dependent dielectric constant, (b) Weibull distribution, and (c) volumetric energy density for neat PTD 3 (solid line), and 1 vol % BZCT nanocomposite (dashed line).

DOI: 10.1021/acsami.5b04158
ACS Appl. Mater. Interfaces 2015, 7, 17819−17825

Table 1. Summary of Parameters Used for Energy Storage Density of Neat PTD3 and 1 vol% Nanocomposite Printed Films

sample	α [MV/cm]	k @ 1 kHz	EDv [J·cm^{-3}]	EDg [Wh·kg^{-1}]
PTD3	4.37	15.71	13.28	3.35
PTD3 + 1 vol % BZCT	0.0926	17.97	36.12	9.09

breakdown is partially attributed to the decrease in film thickness as compared to the spin-coated samples. Avalanche dielectric breakdown can be reduced with a decrease in the material thickness by allowing conducting electrons to reach the anode before achieving a cascade event. Thinner samples also have a greater effective area/volume for heat dissipation, increasing the thermal breakdown slightly.[73−76] Figure 5c shows the energy storage distributions for neat PTD3 and the BZCT nanocomposite. It is clear from the distribution that there is a drastic improvement in the volumetric energy storage capabilities. Table 1 summarizes the parameters to calculate the characteristic energy storage of the neat polymer and nanocomposite film. As can clearly be seen, at the characteristic breakdown field the increase in breakdown strength results in a nearly 3-fold increase of the volumetric and gravimetric energy storage. This increase in breakdown, and therefore energy storage, is not expected to have such a significant increase in highly cross-linked polymer dielectrics. These solutions have a high degree of cross-linking already and would have no added benefit from the cross-linking aspect of the functionalized NPs. At most, it is expected that they would have comparable breakdowns to the neat polymers as, although there is not an increase in cross-linking; the interface is coherent, minimizing defects. If the loading could be increased significantly, then they would have the benefit of no reduction in breakdown but a significant increase in dielectric constant.

4. CONCLUSIONS

High dielectric constant BZCT NPs were functionalized with alkene terminated methoxysilanes in order to covalently attach them into a UV cure, polymer matrix, eliminating the incoherent interface that drastically reduces the breakdown strength of ceramic−polymer nanocomposites. The functionalization procedure produced >70 000 alkene terminated binding sites for polymer attachment as confirmed by TGA and FTIR. Spin-coated samples demonstrated that aggravating the incoherent interface by functionalizing NP with TBAOH led to a 15% decrease in breakdown strength while creating a stronger bond between the particle and matrix, through alkene functionalization, increased the breakdown strength by 17% compared to the neat polymer. This is concluded as having been caused by two factors: (1) improving the interface thereby preventing detrimental charge concentration effects and (2) improving the degree of cross-linking in the material. To prove the potential for high throughput processing, neat polymer and composite films were printed, and it was found that both the breakdown strength and dielectric constant increased, tripling the energy density, from 12 to 36 J·cm^{-3}, compared to the neat polymer films. The advantages given by the photonic curing processing as well as the increased degree of cross-linking allows this approach to be applied to other linear polymer systems that have already demonstrated potential for high energy density dielectric capacitors.

ASSOCIATED CONTENT

Supporting Information

Description of the material; (Figure S1) chemical structures of the monomer solutions used in making the inks; (Figure S2) characterization of structure and stoichiometry for BZCT grown nanoparticles; (Figure S3) SEM and optical images of neat PTD3, BZCT TBAOH-PTD3, and BZCT Alk- PTD3; (Figure S4) 1 cm^2 layers of inkjet printed 1vol% BZCT Alk7-PTD3 nanocomposite, neat PTD3; and (Table S1) calculation of functionalization density for BZCT OL and BZCT OL Alk 7. The Supporting Information is available free of charge on the ACS Publications website at DOI: 10.1021/acsami.5b04158.

AUTHOR INFORMATION

Corresponding Authors

*E-mail: briggs1@tulane.edu.
*E-mail: dchrisey@tulane.edu.

Author Contributions

The manuscript was written through contributions of all authors. All authors have given approval to the final version of the manuscript.

Funding

This work was conducted under the NSF-EFRI-RESTOR #1038272.

Notes

The authors declare no competing financial interest.

ACKNOWLEDGMENTS

Scott M. Grayson and Ravinder Elupula acknowledge support from NSF-CHE 1412439.

ACKNOWLEDGMENTS

The authors would like to acknowledge Vahid Akhavan from Novacentrix (Austin, TX) for his assistance in using the PulseForge tool.

ABBREVIATIONS

NP, nanoparticles
BZCT, (Ba0.7Ca0.3) (Zr0.2Ti0.8)O3
Alk7, 7-octenyltrimethoxysilane
TBAOH, Tetrabutylammonium hydroxide

REFERENCES

(1) Morren, J.; de Haan, S. W. H.; Kling, W. L.; Ferreira, J. A. Wind Turbines Emulating Inertia and Supporting Primary Frequency Control. *IEEE Trans. Power Syst.* **2006**, *21* (1), 433−434.
(2) Short, J. A.; Infield, D. G.; Freris, L. L. Stabilization of Grid Frequency through Dynamic Demand Control. *IEEE Trans. Power Syst.* **2007**, *22* (3), 1284−1293.
(3) Dunn, B.; Kamath, H.; Tarascon, J. Electrical Energy Storage for the Grid: A Battery of Choices. *Science (Washington, DC, U. S.)* **2011**, *334* (6058), 928−935.
(4) Hall, P. J.; Bain, E. J. Energy-Storage Technologies and Electricity Generation. *Energy Policy* **2008**, *36* (12), 4352−4355.
(5) IES; *OECD. Renewable Energy: Medium-Term Market Report 2013*; Paris Cedex 15, France, 2013.

DOI: 10.1021/acsami.5b04158
ACS Appl. Mater. Interfaces 2015, 7, 17819−17825

(6) U.S. DOE. *Annual Energy Outlook 2015 with projections to 2040*; Washington, DC, 2015.
(7) Zervos, A. *Renewables 2013: GLOBAL STATUS REPORT 2013*; 2013.
(8) Yang, H.; Lu, L.; Zhou, W. A Novel Optimization Sizing Model for Hybrid Solar-Wind Power Generation System. *Sol. Energy* **2007**, *81* (1), 76−84.
(9) Vosen, S. R.; Keller, J. O. Hybrid Energy Storage Systems for Stand-Alone Electric Power Systems: Optimization of System Performance and Cost through Control Strategies. *Int. J. Hydrogen Energy* **1999**, *24* (12), 1139−1156.
(10) Wei, Q.; An, Q.; Chen, D.; Mai, L.; Chen, S.; Zhao, Y.; Hercule, K. M.; Xu, L.; Minhas-Khan, A.; Zhang, Q. One-Pot Synthesized Bicontinuous Hierarchical Li3V2(PO4)3/C Mesoporous Nanowires for High-Rate and Ultralong-Life Lithium-Ion Batteries. *Nano Lett.* **2014**, *14* (2), 1042−1048.
(11) Zhang, W.-J. A Review of the Electrochemical Performance of Alloy Anodes for Lithium-Ion Batteries. *J. Power Sources* **2011**, *196* (1), 13−24.
(12) Malini, R.; Uma, U.; Sheela, T.; Ganesan, M.; Renganathan, N. G. Conversion Reactions: A New Pathway to Realise Energy in Lithium-Ion Battery—review. *Ionics* **2009**, *15* (3), 301−307.
(13) Cheng, F.; Chen, J. Metal-Air Batteries: From Oxygen Reduction Electrochemistry to Cathode Catalysts. *Chem. Soc. Rev.* **2012**, *41* (6), 2172−2192.
(14) Aurbach, D.; Gofer, Y.; Lu, Z.; Schechter, a.; Chusid, O.; Gizbar, H.; Cohen, Y.; Ashkenazi, V.; Moshkovich, M.; Turgeman, R. A Short Review on the Comparison between Li Battery Systems and Rechargeable Magnesium Battery Technology. *J. Power Sources* **2001**, *97−98*, 28−32.
(15) Rhodes, K.; Kirkham, M.; Meisner, R.; Parish, C. M.; Dudney, N.; Daniel, C. Novel Cell Design for Combined in Situ Acoustic Emission and X-Ray Diffraction Study during Electrochemical Cycling of Batteries. *Rev. Sci. Instrum.* **2011**, *82* (075107), 1−7.
(16) Papazov, G.; Pavlov, D. Influence of Cycling Current and Power Profiles on the Cycle Life of Lead/acid Batteries. *J. Power Sources* **1996**, *62* (2), 193−199.
(17) Kang, S. J.; Chang, D. H.; U, Y. S. Y. Fatigue and Dielectric Properties of the (Pb, La)TiO3 Thin Films with Various La Concentrations. *Thin Solid Films* **2000**, *373* (1−2), 53−59.
(18) Lee, J. J.; Thio, C. L.; Desu, S. B. Electrode Contacts on Ferroelectric Pb(ZrxTi1-X) O3 and SrBi2Ta2O9 Thin Films and Their Influence on Fatigue Properties. *J. Appl. Phys.* **1995**, *78* (5073), 5073−5078.
(19) Mihara, T.; Watanabe, H.; Araujo, C. P. De. Characteristic Change due to Polarization Fatigue of Sol-Gel Ferroelectric Pb-(Zr0.4Ti0.6)O3 Thin-Films Capacitors. *Japanese J.* **1994**, *33* (9), 5281−5286.
(20) Lawrence, B. *Development of High Energy Density Dielectrics for Pulse Power Applications*; University of Missouri-ROLLA, 2001.
(21) MacDougall, F.; Ennis, J.; Yang, X.; Seal, K.; Phatak, S.; Spinks, B.; Keller, N.; Naruo, C.; Jow, T. Large High Energy Density Pulse Discharge Capacitor Characterization. *2005 IEEE Pulsed Power Conf.* **2005**, 1215−1218.
(22) Chen, X.-Z.; Li, Z.-W.; Cheng, Z.-X.; Zhang, J.-Z.; Shen, Q.-D.; Ge, H.-X.; Li, H.-T. Greatly Enhanced Energy Density and Patterned Films Induced by Photo Cross-Linking of Poly(vinylidene Fluoride-Chlorotrifluoroethylene). *Macromol. Rapid Commun.* **2011**, *32* (1), 94−99.
(23) Gorzkowski, E. P.; Pan, M.-J.; Bender, B. a.; Wu, C. C. M. Effect of Additives on the Crystallization Kinetics of Barium Strontium Titanate Glass−Ceramics. *J. Am. Ceram. Soc.* **2008**, *91* (4), 1065−1069.
(24) Barber, P.; Balasubramanian, S.; Anguchamy, Y.; Gong, S.; Wibowo, A.; Gao, H.; Ploehn, H. J.; zur Loye, H.-C. Polymer Composite and Nanocomposite Dielectric Materials for Pulse Power Energy Storage. *Materials* **2009**, *2* (4), 1697−1733.
(25) Liu, C.; Li, F.; Ma, L.-P.; Cheng, H.-M. Advanced Materials Forenergy Storage. *Adv. Mater.* **2010**, *22* (8), E28−E62.
(26) Arlt, G.; Hennings, D.; de With, G. Dielectric Properties of Fine-Grained Barium Titanate Ceramics. *J. Appl. Phys.* **1985**, *58* (4), 1619.
(27) Lee, H. Y.; Cho, K. H.; Nam, H.-D. Grain Size and Temperature Dependence of Electrical Breakdown in BaTiO 3 Ceramic. *Ferroelectrics* **2006**, *334* (1), 165−169.
(28) Kim, B.-J.; Park, T.-G.; Kim, M.-H. Temperature and Frequency Dependence of Dielectric Properties of (Ba, Sr, Mg) TiO_3 Ceramic Capacitors. *J. Korean Phys. Soc.* **1998**, *32*, 289−292.
(29) Zhao, X.; Evans, J. R. G.; Edirisinghe, M. J.; Song, J. H. Formulation of a Ceramic Ink for a Wide-Array Drop-on-Demand Ink-Jet Printer. *Ceram. Int.* **2003**, *29* (8), 887−892.
(30) Nam, S.; Lee, S.; Lee, Y. Ceramic Processing Research Electrical Properties of the Multilayered PZT/$BaTiO_3$/PZT Thick Films. *J. Ceram. Process. Res.* **2008**, *9* (1), 6−9.
(31) Islam, R. A.; Priya, S. High-Energy Density Ceramic Composition in the System Pb(Zr,Ti)O3- Pb[(Zn,Ni) 1/3 Nb 2/3]O3. *J. Am. Ceram. Soc.* **2006**, *89* (10), 3147−3156.
(32) Yue, Z.; Wang, X.; Zhang, L. Temperature Stable Pb (Zn 1/3 Nb 2/3) O 3-Based Composite Ceramics Prepared by Particle-Coating Method. *J. Mater. Sci. Lett.* **1997**, *16* (16), 1354−1356.
(33) Kamel, T. M.; de With, G. Grain Size Effect on the Poling of Soft Pb(Zr,Ti)O3 Ferroelectric Ceramics. *J. Eur. Ceram. Soc.* **2008**, *28* (4), 851−861.
(34) Ren, P.; Fan, H.; Wang, X.; Liu, K. Effects of Magnesium Doping on Phase Transitions and Dielectric Figure of Merit of Barium Strontium Titanate Ceramics. *Int. J. Appl. Ceram. Technol.* **2012**, *9* (2), 358−365.
(35) Gao, F.; Donf, X.; Mao, C.; Cao, F.; Wang, G. C-a Ratio-Dependent Energy-Storage Density in (0.9−x)Bi0.5Na0.5TiO3−xBaTiO3−0.1K0.5Na0.5NbO3 Ceramics.pdf. *J. Am. Ceram. Soc.* **2011**, *94* (12), 4162−4164.
(36) Yi, D.; Yuan, J.; Liu, H.; Shen, Y.; Lin, Y.-H.; Nan, C.-W.; Xi, X.; He, J. Influence of Al2O3 Additive on the Dielectric Behavior and Energy Density of Ba0.5Sr0.5TiO3 Ceramics. *J. Electroceram.* **2012**, *29* (2), 95−98.
(37) Jiang, S.; Zhang, L.; Zhang, G.; Liu, S.; Yi, J.; Xiong, X.; Yu, Y.; He, J.; Zeng, Y. Effect of Zr:Sn Ratio in the Lead Lanthanum Zirconate Stannate Titanate Anti-Ferroelectric Ceramics on Energy Storage Properties. *Ceram. Int.* **2013**, *39* (5), 5571−5575.
(38) Puli, V. S.; Pradhan, D. K.; Riggs, B. C.; Chrisey, D. B.; Katiyar, R. S. Structure, Ferroelectric, Dielectric and Energy Storage Studies of Ba 0.70 Ca 0.30 TiO 3, Ba(Zr 0.20 Ti 0.80)O 3 Ceramic Capacitors. *Integr. Ferroelectr.* **2014**, *157* (1), 139−146.
(39) Puli, V. S.; Pradhan, D. K.; Riggs, B. C.; Adireddy, S.; Katiyar, R. S.; Chrisey, D. B. Synthesis and Characterization of Lead-Free Ternary Component BST−BCT−BZT Ceramic Capacitors. *J. Adv. Dielectr.* **2014**, *4* (2), 1450014.
(40) Ahmad, Z. In *Dielectric Material*; Silaghi, M. A., Ed.; Intech, 2012; pp 3−26.
(41) Burlingame, Q.; Wu, S.; Lin, M.; Zhang, Q. M. Conduction Mechanisms and Structure-Property Relationships in High Energy Density Aromatic Polythiourea Dielectric Films. *Adv. Energy Mater.* **2013**, *3* (8), 1051−1055.
(42) Chu, B.; Zhou, X.; Neese, B.; Zhang, Q. M. Relaxor Ferroelectric Poly(vinylidene Fluoride-Trifluoroethylene-Chlorofluoroethylene) Terpolymer for High Energy Density Storage Capacitors. *IEEE Trans. Dielectr. Electr. Insul.* **2006**, *13* (5), 1162−1169.
(43) Ishino, I.; Hikita, M.; Suzoki, Y.; Mizutani, T.; Ieda, M. High-Field Conduction and Carrier Traps in Polyethylene Copolymerized with Various Monomers. *Electr. Eng. Japan* **1992**, *112* (7), 1−10.
(44) Li, M.; Stingelin, N.; Michels, J. J.; Spijkman, M.-J.; Asadi, K.; Feldman, K.; Blom, P. W. M.; de Leeuw, D. M. Ferroelectric Phase Diagram of PVDF:PMMA. *Macromolecules* **2012**, *45* (18), 7477−7485.
(45) Meunier, M.; Quirke, N. Molecular Modeling of Electron Trapping in Polymer Insulators. *J. Chem. Phys.* **2000**, *113* (1), 369.

DOI: 10.1021/acsami.5b04158
ACS Appl. Mater. Interfaces 2015, 7, 17819−17825

(46) Park, S.-J.; Cho, K.-S.; Kim, S.-H. A Study on Dielectric Characteristics of Fluorinated Polyimide Thin Film. *J. Colloid Interface Sci.* **2004**, *272* (2), 384−390.
(47) Pawlikowski, G. T. Effects of Polymer Material Variations on High Frequency Dielectric Properties *MRS Online Proc. Libr.* **2009**, *1156*.10.1557/PROC-1156-D02-05
(48) Rabuffi, M.; Picci, G. Status Quo and Future Prospects for Metallized Polypropylene Energy Storage Capacitors. *IEEE Trans. Plasma Sci.* **2002**, *30* (5), 1939−1942.
(49) Rahimabady, M.; Yao, K.; Arabnejad, S.; Lu, L.; Shim, V. P. W.; Cheong Wun Chet, D. Intermolecular Interactions and High Dielectric Energy Storage Density in Poly(vinylidene Fluoride-Hexafluoropropylene)/poly(vinylidene Fluoride) Blend Thin Films. *Appl. Phys. Lett.* **2012**, *100* (25), 252907.
(50) Wang, Y.; Zhou, X.; Lin, M.; Zhang, Q. M. High-Energy Density in Aromatic Polyurea Thin Films. *Appl. Phys. Lett.* **2009**, *94* (20), 202905.
(51) Wu, S.; Li, W.; Lin, M.; Burlingame, Q.; Chen, Q.; Payzant, A.; Xiao, K.; Zhang, Q. M. Aromatic Polythiourea Dielectrics with Ultrahigh Breakdown Field Strength, Low Dielectric Loss, and High Electric Energy Density. *Adv. Mater.* **2013**, *25* (12), 1734−1738.
(52) Popielarz, R.; Chiang, C. K.; Nozaki, R.; Obrzut, J. Dielectric Properties of Polymer/Ferroelectric Ceramic Composites from 100 Hz to 10 GHz. *Macromolecules* **2001**, *34* (17), 5910−5915.
(53) Arbatti, M.; Shan, X.; Cheng, Z.-Y. Ceramic−Polymer Composites with High Dielectric Constant. *Adv. Mater.* **2007**, *19* (10), 1369−1372.
(54) Popielarz, R.; Chiang, C. K. Polymer Composites with the Dielectric Constant Comparable to that of Barium Titanate Ceramics. *Mater. Sci. Eng., B* **2007**, *139* (1), 48−54.
(55) Zhou, Y.; Zhang, Q.; Luo, J.; Tang, Q.; Du, J. Structural and Dielectric Characterization of Gd2O3-Added BaO−Na2O−Nb2O5−SiO2 Glass−ceramic Composites. *Scr. Mater.* **2011**, *65* (4), 296−299.
(56) Bai, Y.; Cheng, Z.-Y.; Bharti, V.; Xu, H. S.; Zhang, Q. M. High-Dielectric-Constant Ceramic-Powder Polymer Composites. *Appl. Phys. Lett.* **2000**, *76* (25), 3804.
(57) Barber, P.; Pellechia, P. J.; Ploehn, H. J.; zur Loye, H.-C. High-Dielectric Polymer Composite Materials from a Series of Mixed-Metal Phenylphosphonates, ATi(C6H5PO3)3 for Dielectric Energy Storage. *ACS Appl. Mater. Interfaces* **2010**, *2* (9), 2553−2559.
(58) Zhou, T.; Zha, J.-W.; Cui, R.-Y.; Fan, B.-H.; Yuan, J.-K.; Dang, Z.-M. Improving Dielectric Properties of BaTiO3/ferroelectric Polymer Composites by Employing Surface Hydroxylated BaTiO3 Nanoparticles. *ACS Appl. Mater. Interfaces* **2011**, *3* (7), 2184−2188.
(59) Su, X.; Riggs, B. C.; Tomozawa, M.; Nelson, J. K.; Chrisey, D. B. Preparation of BaTiO 3 /Low Melting Glasses Core-Shell Nanoparticles for Energy Storage Capacitor Applications. *J. Mater. Chem. A* **2014**, *2*, 18087−18096.
(60) Puli, V. S.; Riggs, B. C.; Grayson, S. M.; Katiyar, R. S.; Chrisey, D. B. Surface Modified BaTiO 3 -Polystyrene Nanocomposites for Energy Storage. *Int. J. Nanotechnol.* **2014**, *11* (9/10/11), 910−920.
(61) Ejaz, M.; Puli, V. S.; Elupula, R.; Adireddy, S.; Riggs, B. C.; Chrisey, D. B.; Grayson, S. M. Core-Shell Structured Poly(glycidyl methacrylate)/BaTiO 3 Nanocomposites Prepared by Surface-Initiated Atom Transfer Radical Polymerization: A Novel Material for High Energy Density Dielectric Storage. *J. Polym. Sci., Part A: Polym. Chem.* **2015**, *53* (6), 719−728.
(62) Li, J.; Seok, S. I.; Chu, B.; Dogan, F.; Zhang, Q.; Wang, Q. Nanocomposites of Ferroelectric Polymers with TiO 2 Nanoparticles Exhibiting Significantly Enhanced Electrical Energy Density. *Adv. Mater.* **2009**, *21* (2), 217−221.
(63) Chu, B.; Lin, M.; Neese, B.; Zhang, Q. Interfaces in Poly(vinylidene Fluoride) terpolymer/ZrO[sub 2] Nanocomposites and Their Effect on Dielectric Properties. *J. Appl. Phys.* **2009**, *105* (1), 014103.
(64) Yuan, J.-K.; Dang, Z.-M.; Yao, S.-H.; Zha, J.-W.; Zhou, T.; Li, S.-T.; Bai, J. Fabrication and Dielectric Properties of Advanced High Permittivity Polyaniline/poly(vinylidene Fluoride) Nanohybrid Films with High Energy Storage Density. *J. Mater. Chem.* **2010**, *20* (12), 2441.
(65) Yang, Y.; Wang, Z.; Ding, Y.; Lu, Z.; Sun, H.; Li, Y.; Wei, J.; Xiong, R.; Shi, J.; Liu, Z.; Lei, Q. Research Update: Polyimide/CaCu3Ti4O12 Nanofiber Functional Hybrid Films with Improved Dielectric Properties. *APL Mater.* **2013**, *1* (5), 050701.
(66) Yang, K.; Huang, X.; Huang, Y. Fluoro-Polymer@ BaTiO3 Hybrid Nanoparticles Prepared via RAFT Polymerization: Toward Ferroelectric Polymer Nanocomposites with High Dielectric Constant and. *Chem. Mater.* **2013**, *25* (11), 2327−2338.
(67) Tang, H.; Sodano, H. Ultra High Energy Density Nanocomposite Capacitors with Fast Discharge Using Ba0. 2Sr0. 8TiO3 Nanowires. *Nano Lett.* **2013**, *13* (4), 1373−1379.
(68) Wang, C.; Lee, W.-Y.; Nakajima, R.; Mei, J.; Kim, D. H.; Bao, Z. Thiol−ene Cross-Linked Polymer Gate Dielectrics for Low-Voltage Organic Thin-Film Transistors. *Chem. Mater.* **2013**, *25* (23), 4806−4812.
(69) Riggs, B. C.; Elupula, R.; Grayson, S. M.; Chrisey, D. B. Photonic Curing of Aromatic Thiol-Ene Click Dielectric Capacitors via Inkjet Printing. *J. Mater. Chem. A* **2014**, *2* (41), 17380−17386.
(70) Ko, J. M.; Kang, Y. H.; Lee, C.; Cho, S. Y. Electrically and Thermally Stable Gate Dielectrics from Thiol−ene Cross-Linked Systems for Use in Organic Thin-Film Transistors. *J. Mater. Chem. C* **2013**, *1* (18), 3091.
(71) Adireddy, S.; Lin, C.; Cao, B.; Zhou, W.; Caruntu, G. Solution-Based Growth of Monodisperse Cube-Like BaTiO 3 Colloidal Nanocrystals. *Chem. Mater.* **2010**, *22* (6), 1946−1948.
(72) Yuan, X.; Chung, T. C. M. Cross-Linking Effect on Dielectric Properties of Polypropylene Thin Films and Applications in Electric Energy Storage. *Appl. Phys. Lett.* **2011**, *98* (6), 062901.
(73) Ieda, M. Dielectric Breakdown Process of Polymers. *IEEE Trans. Electr. Insul.* **1980**, *EI−15* (3), 206−224.
(74) Dissado, L. A.; Fothergill, J. C. *Electrical Degradation and Breakdown in Polymers*; Stevens, G. C., Ed.; The Institution of Engineering and Technology, 1992.
(75) Reddy, C. C.; Ramu, T. S. Polymer Nanocomposites as Insulation for HV DC Cables - Investigations on the Thermal Breakdown. *IEEE Trans. Dielectr. Electr. Insul.* **2008**, *15* (1), 221−227.
(76) Allcock, R.; Cook, W. J. The Thermal Breakdown of Poly (Diphenoxyphosphazene) lY2. *Macromolecules* **1974**, *7* (5), 571−575.

DOI: 10.1021/acsami.5b04158
ACS Appl. Mater. Interfaces 2015, 7, 17819−17825